Design, Qualification, Manufacturing and Integration of IXV Ablative Thermal Protection System.

Cioeta Mario, Di Vita Gandolfo**, Signorelli Maria Teresa***, Bianco Gianluca*, Cutroni Maurizio*, Damiani Francesco*, Ferretti Viviana* and Rotondo Adriano**

**AVIO S.p.A.*

**Via Ariana, Km 5.2 00034 Colleferro (RM), Italy*

***ESA-HQ*

***Daumesnil, 52 rue Jacques Hillairet - 75012 Paris France*

**** Thales Alenia Space Italia S.p.A.*

**** Strada Antica di Collegno 253 - 10146 Torino, Italy*

Abstract

In the present paper, all the activities carried out by Avio S.p.A in order to define, qualify, manufacture and integrate the IXV Ablative TPS will be presented.
In particular the extensive numerical simulation in both small and full scale testing activities will be overviewed.
Wide-ranging testing activity has been carried out in order to verify, confirm and correlate the numerical models used for TPS sizing. Tests ranged from classical thermo-mechanical characterization traction specimens to tests in plasma wind tunnels on dedicated prototypes.
Finally manufacturing and integration activities will be described emphasizing technological aspects solved in order to meet the stringent requirements in terms of shape accuracy and integration tolerances.

1. Introduction

The IXV project is designed to develop and flight-test the technologies and critical systems for Europe's future autonomous controlled reentry for return missions from low Earth orbit.
The Prime Contractor for IXV flight segment and ground segment is Thales Alenia Space Italia, supported by about 40 other European companies, universities and research institutes.

Figure 1: IXV Vehicle during recovery immediately after its suborbital flight.

ESA's Intermediate eXperimental Vehicle flew a flawless reentry and splashed down in the Pacific Ocean just west of the Galapagos islands.
The IXV spaceplane lifted off at 13:40 GMT (14:40 CET, 10:40 local time) on 11 February from Europe's Spaceport in Kourou, French Guiana atop a Vega rocket. It separated from Vega at an altitude of 340 km and continued up to

412 km. Reentering from this suborbital path, it recorded a vast amount of data from more than 300 advanced and conventional sensors.

2. The Ablative TPS

The Ablative Thermal Protection System is part of the Intermediate Experimental Vehicle (IXV). It has been introduced in order to protect the structure of IXV from the effects of the thermal environment starting from the stand-by on ground phase, up to the atmospheric re-entry and descent phases.
Ablative TPS provides the required insulation characteristics, both during stand-by on ground and flight phase.
It protects the IXV cold structure from the external thermal environment effects and from the attack of atmospheric agents. Ablative TPS is made of several different materials depending on the peculiarity of the function and of the component to be protected. The main constituent is a cork based material named P50 which is coated on the external surface with an antistatic paint, that avoids electrostatic charge accumulation and provides known thermo-optical properties to the outer surface when it is not subjected to thermoablative degradation.
The main sub-assemblies of IXV ablative TPS are the following (See Figure 2):

- Leeward Assembly
- Lateral Assembly
- Base Assembly

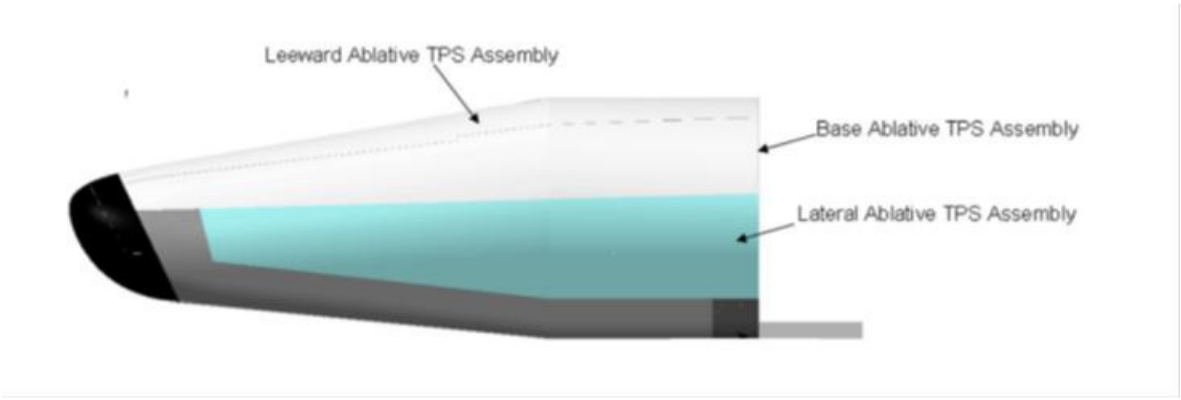

Figure 2: IXV Ablative TPS Main Sub-Assemblies

On its turn, each of the above sub-assemblies is composed of several parts with different function. At the end, the whole ablative TPS is composed of more than 700 tiles of thermal protection material.

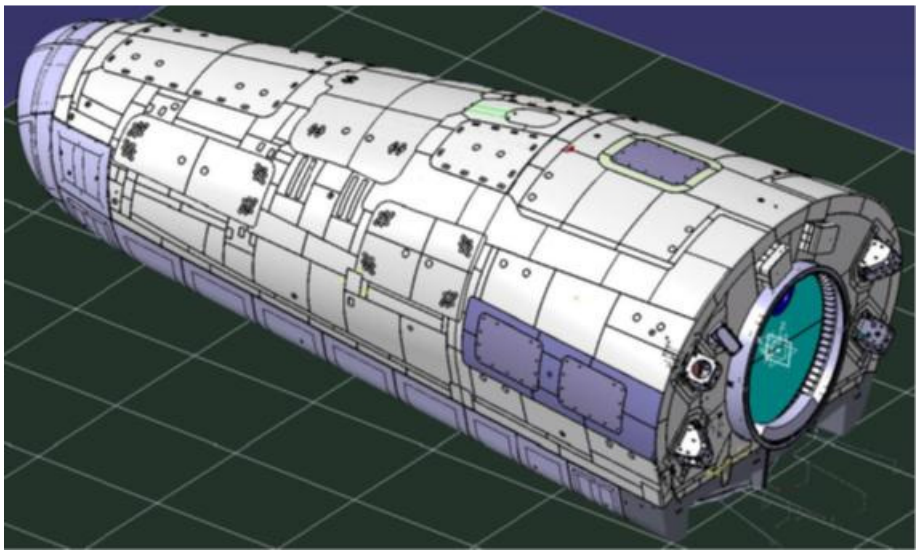

Figure 3: IXV Ablative TPS definition

The actual ablative TPS tiles distribution is reported in the previous figure.

Two materials are used for the ablative TPS:

- A cork based material with very high thermal insulating performance
- A silicone based material for covering antennas and electronic devices in order to assure radio transparency for ground to spacecraft communications.

The TPS tiles are bonded on the spacecraft cold structure by means of different high strength adhesives depending on the interface characteristics. Considering that the cold structures surface where the TPS tiles have to be bonded is made of several materials (CFRP, titanium alloys, aluminium alloys) with different surface finishing and treatment, more than ten different bonded interfaces needed to be characterised and qualified.

3. Thermal dimensioning

The flight mission thermal analysis has been performed using a lumped parameter numerical code able to take into account effects of material ablation where the in-depth temperature of protection layer is higher than the decomposing temperature. In this case together with the standard Fourier equation, the code solves the equations modelling the thermal decomposition process of an ablating material (Arrhenius low model).

$$\left(\frac{\partial \rho_i}{\partial \theta}\right) = -B_i \exp\left(\frac{-E_{a_i}}{RT}\right) \rho_{0_i} \left(\frac{\rho_i - \rho_{r_i}}{\rho_{0_i}}\right)^{\psi_i} \quad (1)$$

Where ρ_{ri} is the residual density of the component i and ρ_{0i} is the original density of the same component i. The values ρ_{0i} ρ_{ri} B_i ψ_I and E_{ai} are input paramethers for the main material.
Decomposition reactions are based on a three-component model. The back-wall of the composite material may transfer energy by convection and radiation. The ablating surface boundary conditions may take one of three forms:

- General convection-radiation heating with coupled mass transfer, using a transfer coefficient approach, including the effects of unequal heat and mass transfer coefficients (non-unity Lewis number) and unequal mass diffusion coefficients. Surface thermo chemistry computations need not presume chemical equilibrium at the surface, but can account for kinetic effects, and can also consider thin layer melting or failing.
- Specified surface temperature and surface recession rate
- Specified radiation view factor and incident radiation flux, as function of time, for a stationary surface.

Any combination of options may be used for a single computation.
The input data needed to perform the thermal analysis with lumped parameter numerical model are mainly of three types:

- thermal loads on the external surface of the heated material;
- thermo-physical characteristics of the materials;
- the thermal interface of IXV cold structure with the internal environment;

In the most loaded regions the sizing heat flux reaches values of more than 150 000 W/m^2 during the hottest re-entry phase.
The TPS thermal design has been carried out by analysing some discrete control points with the model described above. The location of control points, in particular those of interest for the ablative TPS is given hereafter and depicted in the following Figure 4. Among the control points, those driving the TPS sizing are:

- B2 for base
- L5N for leeward
- LS9 for lateral

The Ablative TPS sizing control point, together with the thermal protection thickness installed and the allowable temperature at Ablative TPS / cold structure interface are reported in **Table 1**. The maximum temperature during mission phase are reported in the same table, in order to justify the Ablative TPS sizing.

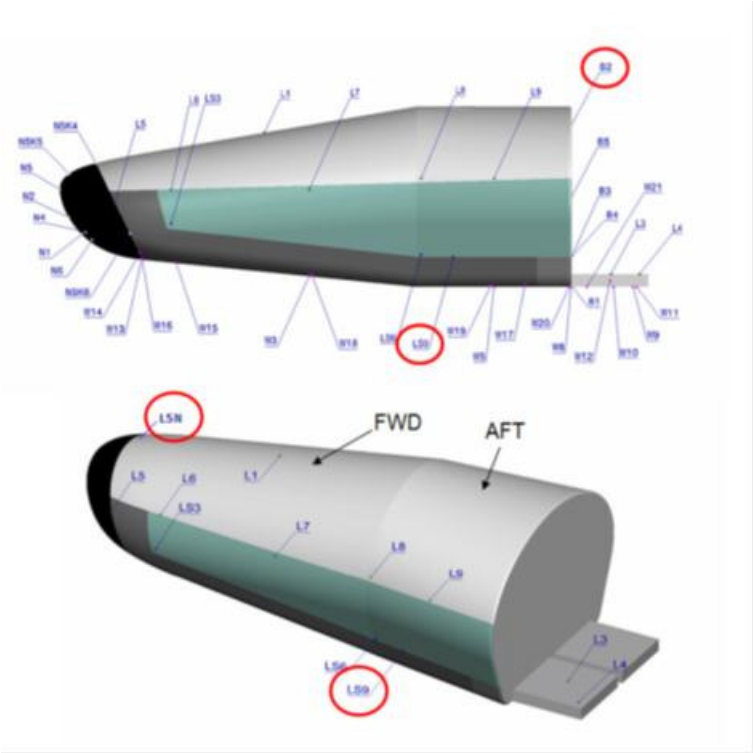

Figure 4: TPS Thermal Control Points

Leeward L5N control point is subjected to heat flux about one half compared to lateral LS9 control point. The effect of different thermal load are hereafter resumed:

- maximum surface temperature is about 950 °C on lateral, about 750°C on leeward.
- erosion is 1.5 mm for lateral, is 0 for leeward.
- decomposed thickness is 7.7 mm for lateral, 8.4 for leeward

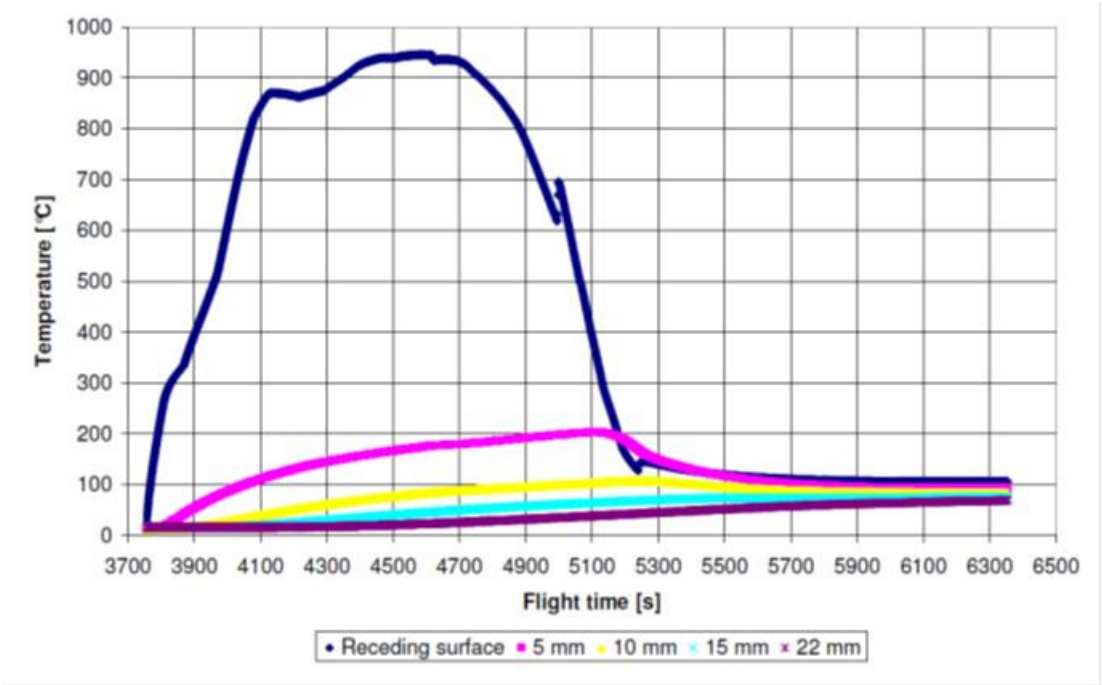

Figure 5: Temperature distribution through thickness on Lateral assembly.

As an example, in the previous Figure 5: Temperature distribution through thickness on Lateral assembly. the temperature field through the ablative TPS thickness is shown on lateral assembly which the region where the highest temperatures are reached.
Combined effect of lower surface temperature without erosion but higher degraded thickness (leeward) and higher surface temperature with ablation and lower degraded thickness (lateral) provides similar temperatures at backwall. Anyway since P50 is an effective insulating material, thermal gradient is very high and it is located immediately below the heated surface. Most of material thickness is still virgin, therefore backwall temperature (especially when thickness is quite consistent as in lateral and leeward cases) is not greatly influenced on external heat flux.

Table 1: Summary Table of ablative TPS temperatures on IXV Assemblies.

	Control Point ID	**Ablative TPS Material**	**Ablative TPS Thickness [mm]**	**Admissible Temperature on cold Structure [°C]**	**Max Temperature at Cold Structure Interface [°C]**
Leeward Assembly	L5N	P50	22.0	160.0	67.0
Lateral assembly	LS9	P50	22.0	160.0	69.1
Base Assembly	B2	P50	18.0	160.0	30.8

A sensitivity analysis has been performed in order to assess the impact of variation range of P50 thermal properties, the ablation parameters and the formation enthalpy of char.

4. Structural dimensioning

All the components of the ablative TPS have been analysed in order to verify their ability to withstand the loads imposed during the ascent and re-entry phases.

Particular attention shall be paid to those tiles presenting some unglued areas. This is the case of tiles covering specific areas of the cold structure such as the parachute jettisoning panels and the parachute bridles.

For these components a specific analysis logic has been set up.

In order to verify the capability of the IXV thermal protection to survive to the dynamic environment during the entire mission, the thermal protection has to be able to withstand the following loads:

Sine Loads in the range 5Hz – 100Hz

QSL Loads

Shock loads

The verification has been done by analytical and numerical methods using simplified models whenever possible and in the most critical cases a FEM approach has been used.

Concerning the shock loads, considering the mechanical behaviour with high damping ratio of P50 material shock is not dimensioning for this kind of verification.

SINE LOADS 5HZ – 100HZ

Such environment is relevant if the resonance peaks of the component are within the test range. If no peak is inside this range the low frequency environment is not the critical one.

Due to the high number of configuration to be analysed the following logic has been used:

1. Using an analytical approach the first eigen-frequency of the most critical configuration has been calculated.

2. If the first frequency (calculated with the analytical approach) is under the 100Hz a FEM is built and analysed in order to verify if the more accurate numerical model confirms the resonance peak is inside the test range:

a. If the FEM confirms the peak is in the test range the amplification factor is calculated and the capability of the part considered to withstand the loads is verified

b. If no resonance peak is present in the frequency range no further investigation is done.

Most critical configuration (the frequency of the first mode) is selected and analysed and a worst case enveloping the remaining ones is selected. The analytical formulas use is reported in the figure hereunder for a uniform load w per unit area including own weight:

$$f = \frac{K_1}{2\pi}\sqrt{\frac{Dg}{wa^4}} \tag{2}$$

Where *K1* is tabulated for various ratios of *a/b*.

Table 2: Natural frequencies of vibration for rectangular plate; all edges fixed [A.D.1]

a/b	**1**	**0.9**	**0.8**	**0.6**	**0.4**	**0.2**	**0**
K_1	36.0	32.7	29.9	25.9	23.6	22.6	22.4

The most critical configuration is the one with 0.172 m of cantilever cork, 0.384mm wide with 8.5mm engravings. In this case the load carrying thickness is equal to 6.5mm.

Applying the formula above in the first natural frequency is : 30Hz

The base corner configuration identified as critical from the first natural frequency (30 Hz analytically determined) has been analyzed by 3D FEM.

As expected the first frequency is very much higher than calculated under the previous conservative assumption. The first eigen-frequency calculated by FEM resulted to be 97.5 Hz. In the next figure the shape and the frequency of the first mode is shown.

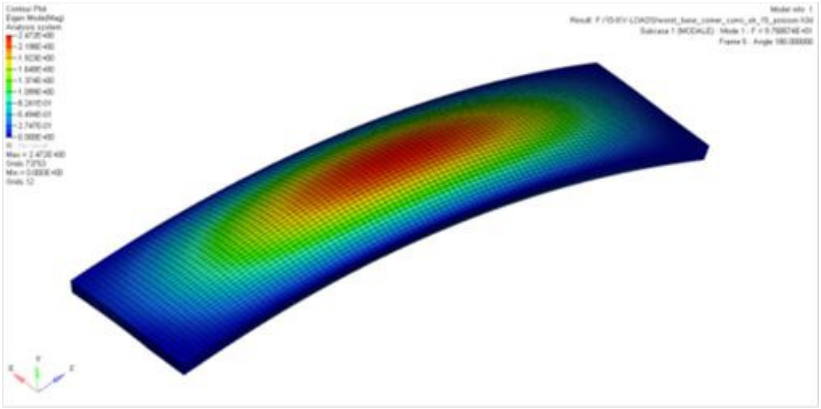

Figure 6: First mode shape and frequency

Even if no additional analysis should be necessary, due to the fact that the 97.5Hz, is very close to the upper limit of the frequency range of interest, and has been evaluated assuming the minimum young modulus (evaluate at 99% of probability and 50% of confidence) the FRF and the stress pattern due to the qualification levels (see [A.D.1]) have been calculated.

The amplification factor has been calculated on the three directions for both the excitation direction and the acceleration response is taken in the middle of the tile where the amplification factor is the highest.:

- IXV axial direction;
- IXV lateral direction;

The response in axial direction is constant and at the end of the frequency range of interest the amplification is 1.04, the load imposed at the base is the same seen from the tile.

On the other hand the lateral response when exciting in axial direction is very low. In correspondence of the mode the mode at 97 Hz and the amplification factor is less than 0.045.

As expected the lateral direction excitation amplification factor is the highest one and it is in correspondence of the mode at 97Hz. The lateral direction response with lateral direction excitation amplification factor is 7. In turn, the axial direction response with lateral direction excitation is very low. A very small coupling between the lateral and axial direction is present.

In the next figure the Von Mises stress pattern is shown for the lateral direction excitation which is the highest one.

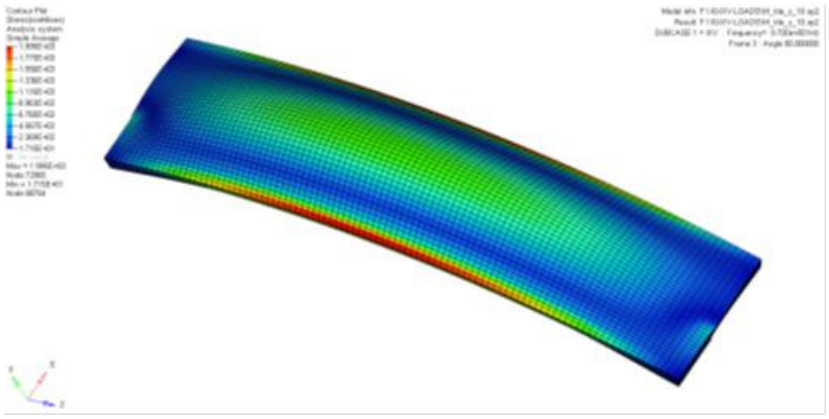

Figure 7: Stress pattern lateral direction excitation

In fact the excitation direction and the mode shape are “aligned”. The Max Von Mises stress is at 97 Hz: 1995Pa (the excitation level is 1 m/s^2). Considering the input level of 30.6g the maximum stress is 306 times 1995 Pa equal to 0.61E+6 Pa. It is important to underline that the high stress values are in correspondence of the edge where the boundary condition are applied. Despite this, the maximum stress is well under the ultimate pull strength 1Mpa (80°C).

QUASI STATIC LOADS

Such environment is relevant in terms of stress inside the thermal protection. The biggest part of it is bonded to the lower structure being in this way supported and for this reason able to transfer the load to the lower part. Also in this case the most critical zones of the thermal protection are the unbonded parts.

Due to the high number of configuration to be analyzed the following logic has been used:

- Use of an analytical approach to identify the maximum stress (compression and tension) in the material for the most critical zones
- If the stress (calculated with the analytical approach) is very close to the ultimate stress then a FEM approach will be used.

Considering the very different configurations present the following conservative assumption are considered valid for the calculation of the stress:

Table 3: dimensioning QSL loads

Load Event	**Longitudinal Load [g]**	**Lateral Load [g]**
Lift Off	-5.25/+0.75	±1.35
Max Dynamic pressure	-4.5/-3.0	±1.35
1st stage Max Acceleration	-7.5/-6.0	±1.35
2nd stage Max Acceleration	-7.1/-6.5	±1.35
3rd stage Max Acceleration	-7.5/+4.5	±1.35

The axial quasi static load, 7.5 g, is not considered critical. Due to the very low density of the cork (500 Kg/m^3), the compression loads induced by the mass of the unbounded part of the thermal protection is very low. Moreover the in this case the cork is compressed as an axial spring under its own weight.

The critical loads are the one applied normal to the tile plane, 1.35 g. In fact in the zones above highlighted (unbonded areas), the off plane quasi static loads induce a flexural deformation with zones of compression an tension:

Far from the constraints the stress field is considered purely induced by the flexural deformation and the formulas here under reported are used:

8. Rectangular plate, all edges fixed

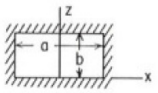

8a. Uniform over entire plate

(At center of long edge) $\text{Max } \sigma = \frac{-\beta_1 q b^2}{t^2}$

(At center) $\sigma = \frac{\beta_2 q b^2}{t^2}$ and $\max y = \frac{\alpha q b^4}{E t^3}$

a/b	1.0	1.2	1.4	1.6	1.8	2.0	∞
β_1	0.3078	0.3834	0.4356	0.4680	0.4872	0.4974	0.5000
β_2	0.1386	0.1794	0.2094	0.2286	0.2406	0.2472	0.2500
α	0.0138	0.0188	0.0226	0.0251	0.0267	0.0277	0.0284

Figure 8 Formulas for flat plates with straight boundaries constant thickness [A.D.1]

The most critical configuration will be the plates where the edges are more distant for two reason:

- The extension of the cantilever is higher so the stress will be higher;
- The mass, so the load, generated by the QSL acceleration is higher;

In all the cases analysed with the analytical model the highest stress is well under the thermal protection material allowable strength that is 1 Mpa. The Margin of Safety in all the analysis ranges from 45 to more than 1000. No criticality is evidenced and no further refined analysis have been necessary.

5. Testing Activity

A wide testing activity has been carried out in order to verify, confirm and correlate the numerical models used for TPS sizing. The used materials have been characterized form the mechanical, thermal, ablative and chemical compatibility point of view. Tests have been performed in several European test facilities including CIRA, University of Naples, University of Rome, DLR and VKY institutes. Tests ranged from classical thermo-mechanical characterization traction specimen to very peculiar test in plasma wind tunnels on dedicated breadboards and prototypes.
Main testing areas were:

- Material properties characterization
- Aerothermal tests to verify ablative performance of TPS material
- Prototype testing for mechanical and environmental behavior verification
- Full scale testing for manufacturing and integration processes verification and implementation

In the next paragraphs an overview of the performed test will be given.

MATERIAL TESTING

All the materials used in the ablative TPS have been tested for determination of critical parameters to be used in the numerical analyses and of allowable values to be used in the design verification.

Following test have been performed:

- material composition
- thermophysical tests
- mechanical characterization
- interface tests
- shock, sine & random tests
- humidity tests
- ageing tests
- outgassing tests
- torch test

Most of the quantitative results of these tests are reserved and cannot be disclosed outside the project. However in the next pictures and description some of the tested items and test setup are presented.

First of all, mechanical properties of all the materials have been tested with particular attention to the bonded interface behavior and strength. For each interface, a test campaign has been carried out with specimen tested at low and high temperatures and with traction and shear specimen.

In the next figures the typical specimens tested for interface strength determination are shown. As can be seen the success criteria for all the tests is that the rupture shall occur in the thermal insulation material and not in correspondence of the interface between the TPS material and the adhesive or the adhesive and the cold structure material.

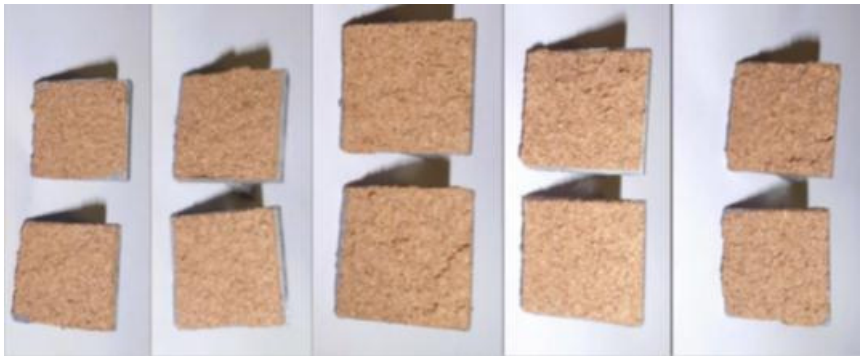

Figure 9 Tension Specimens

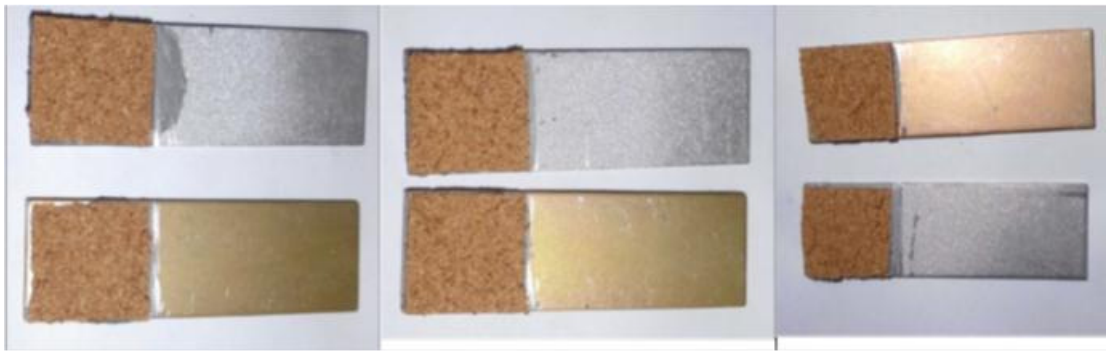

Figure 10 Shear Specimens

In order to verify the capability of TPS materials to withstand the low frequency sinusoidal excitations, the envelope spectrum of noise and the shock loads at TPS tile level and interface level, three different tests have been performed.

The success criteria, which certificate that the P50 is able to withstand the aforementioned loads, is that no degradation occurs during test at P50 tile level and at P50 interface level.

Test configuration lay-up components are listed hereafter:

For sinus and random vibration

- Shaker;
- accelerometers to measure the load at thermal protection interface;
- an electronic system to acquire the accelerations;

For shock test

- Shock machine (BERTA or hammer);
- shock accelerometer to measure the load at thermal protection interface;
- an electronic system to acquire the accelerations.

In the next pictures the item under tests are shown.

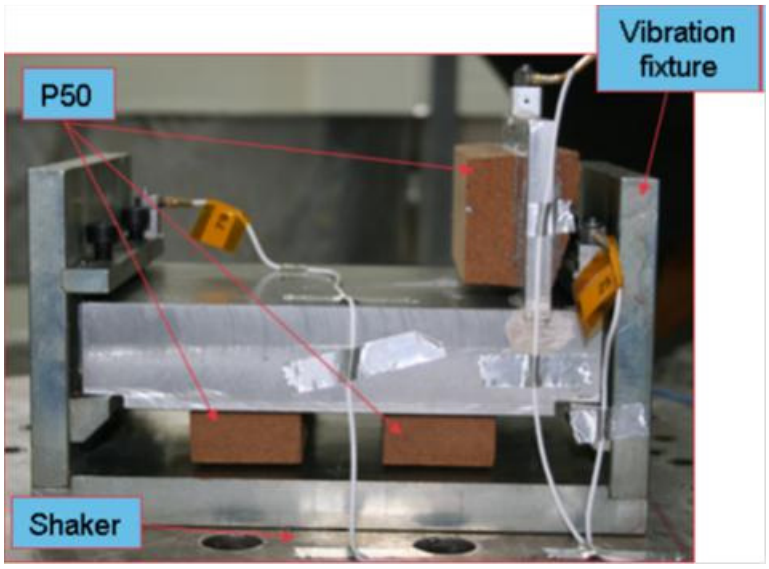

Figure 11: test configuration adopted for sinusoidal and random tests

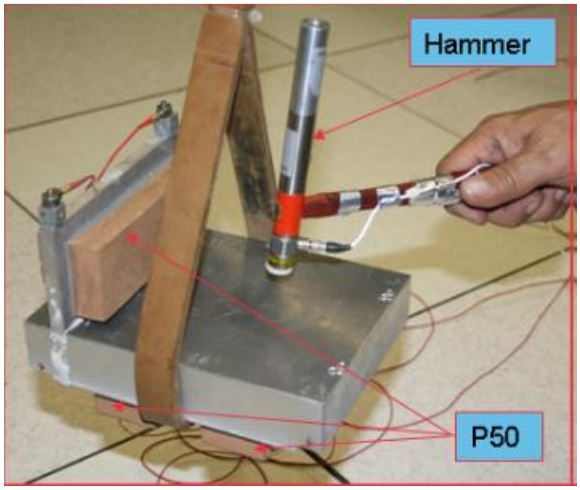

Figure 12: test configuration adopted for shock tests

In order to quantify the TPS behavior under the effect of humidity environment a dedicated humidity intermitting test has been performed. During the humidity intermitting test the TPS samples have been alternatively exposed to Kourou environmental conditions and to storage environmental conditions:

Storage conditions:

- Hour =20
- T = 21 °C
- Humidity = 65%

Launch pad conditions:

- Hour =14;
- T = 34 °C;
- Humidity = 95%;

The aim of this test is to evaluate the eventual humidity absorption and release. This is particularly a critical aspect for the P50 material that being based on cork granulate is quite sensitive to humid environment.

AEROTHERMAL TESTS

Extensive testing in plasma environment have been carried out in order to select and characterize the candidate materials for ablative TPS manufacturing. Particular attention during these test has been put on the behavior of ablative material when exposed to very high heat fluxes typical of an atmospheric reentry. Mai evaluated aspects are:

- presence of grooves on external charred layer;
- consistency and stability of the charred layer
- sensible lateral heating samples;
- swelling of ablative material;

Tests have been performed at the VKI Plasmatron in order to verify the robustness of the ablative TPS design and to compare data with previous test results. Such test campaign, to be performed in order to:

- reproduce completely boundary conditions expected during IXV flight
- reproduce conditions tested on specimens in previous test campaign

is mainly focused on the flat plate configuration (3 runs with two repetitions have been conducted on this set-up in order to characterize material from thermal ablative point of view, 2 runs with repetitions on similar set up in order to characterize material interfaces), but a short experimental investigation has been also performed on the stagnation configuration (1 run with repetitions has been conducted on embedded set-up, 1 run with repetitions has been conducted on hemispherical set-up).

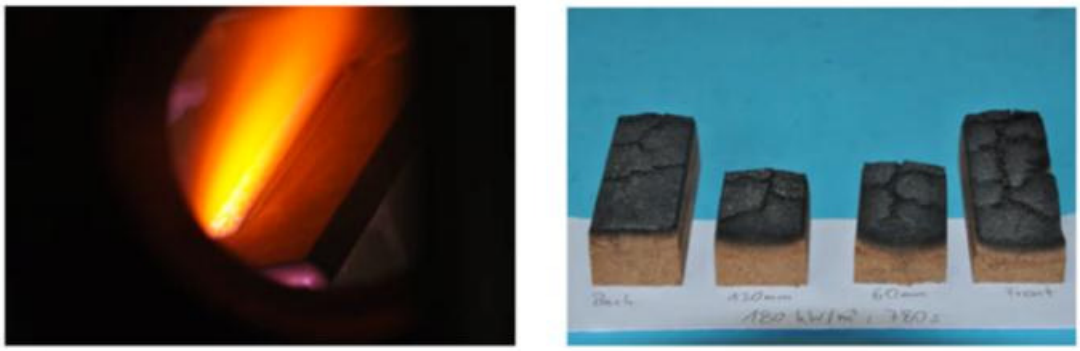

Figure 13: Flat plate test – 180Kw/m2

Figure 14: Hemispherical tests – 330s

From a qualitative analysis of the experimental results it is possible to conclude that for:
Silicone based ablative materials present

- No compact char layer
- No Ablation
- No mechanical erosion
- Swelling

Cork based ablative materials present

- Very compact char layer
- Ablation
- No mechanical erosion
- No swelling

For this reason has been decided to use cork based ablative material for IXV TPS manufacturing since it presents much better dimensional stability and charred layer consistency. Silicone based ablative material has been used for

the region where radio transparency is needed (antennas, radar, …) also due to the fact that thermal fluxes in these region are lower.

PROTOTYPE AND FULL SCALE TESTS

After having selected and characterized the material at specimen level, several large scale test have been carried out in order to verify the effectiveness and the reliability of the technological process for the complete integration of the IXV ablative TPS.
The most critical aspects to solve were:

- Very high number of parts to be integrated
- Integration sequence taking into account IXV spacecraft AIT constraints
- Bonding processes with different adhesives on different cold structure surfaces
- Correct behavior of TPS tile in zone with peculiar functioning (jettison panels, parachute bridles, umbilical connection sealing, removable AIT panels).
- Very stringent requirements in terms of spacecraft outside surface accuracy, gap precision among the tiles and double curvature shape reproducing.
- Macroscopic behavior of ablative TPS sub-system under IXV system environmental testing

On fully representative section of the spacecraft, several integration processes have been tested such as vacuum bagging sensor integration, repair procedure implementation and unbonded area verification. In the next picture a comparison between the 3D model and the realized item is shown.

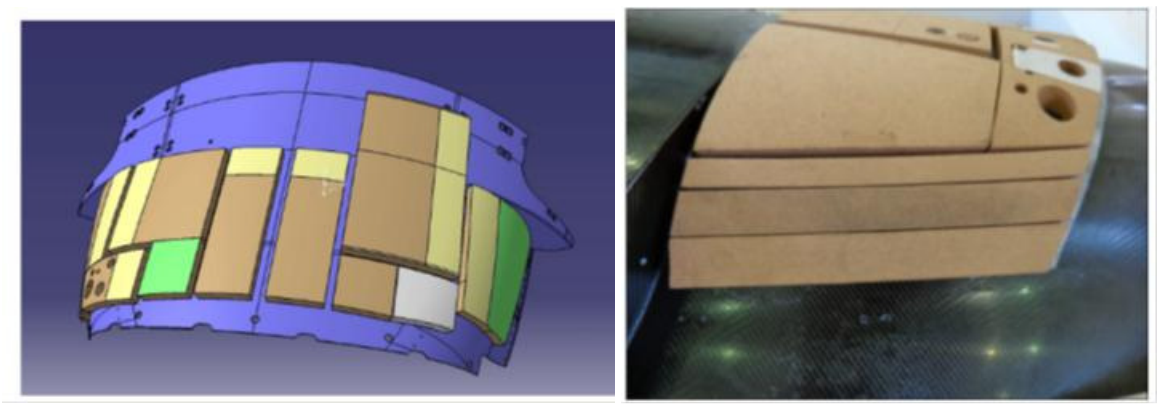

Figure 15: IXV full Scale Mock up as design and as built.

Another important test has been the umbilical cover closure test. In this test performed in thermal-vacuum environment, the functionality of the TPS to seal the umbilical connector after IXV spacecraft separation from the VEGA launch Vehicle has been verified. In the following picture the test item is shown before the test execution and after having completed several opening and closure tests and having been submitted to several thermal-vacuum cycles.

Figure 16: Umbilical connectors cover before and after qualification testing campaign.

6. Flight Model Integration

IXV TPS flight model integration took place in several sites following the evolution and movements of IXV spacecraft along its whole life.
First ablative TPS integration activities have been carried out in Turin at Thales Alenia Space S.p.A premises. Here the first tiles have been integrated on the cold structure.

Figure 17: first integrated tiles of IXV ablative TPS.

At this step of integration most of the tiles of lateral, upper and base assemblies have been integrated.

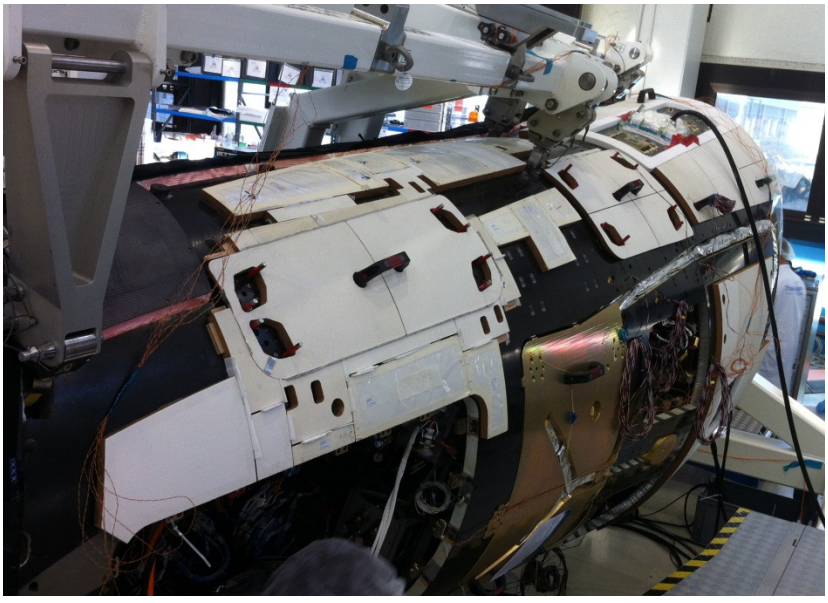

Figure 18: Jettison and lateral assembly integrated in Italy

Then flight model has been moved to ESA-ESTEC premises in Netherlands for environmental testing and further parts of ablative have been integrated. In particular parachute and other lateral panels tiles have been finalised as long as the tiles interfacing with hot temperature TPS on the bottom side of the spacecraft.

Whenever it is possible, vacuum bagging integration process has been used being the most reliable and robust one. However due to logistic and accessibility constraints, for integrating some of the parts, specific tools have been developed in order to keep the tiles in the right position and apply the correct pressure on the external surface for the time necessary for the adhesive polymerisation.

Last step of the integration has been carried out directly at the Guyane Space Centre during the spacecraft preparation for the launch campaign. In particular in this phase, the operation of filling all the gaps between the installed tiles with specific fillers has been carried out in order to assure a complete tightness of the ablative TPS with respect to external aerothermal environment.

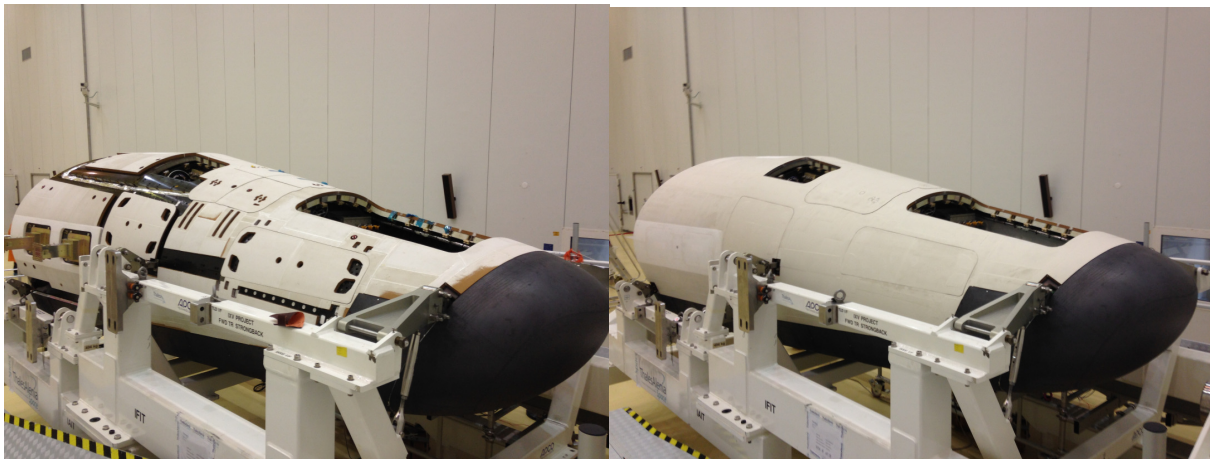

Figure 19: IXV Spacecraft before and after tiles gap filling and external painting finishing

In this phase the external antistatic paint has been applied among the ablative TPS tiles in order to restore the electrical continuity of the spacecraft external surface.

The last tiles of the ablative TPS, has been installed immediately before the installation of the spacecraft on the VEGA launch vehicle payload adapter a few days before the launch. These are the tiles covering the attachment of the spacecraft with the ground support equipment, and are the last components installed on IXV.

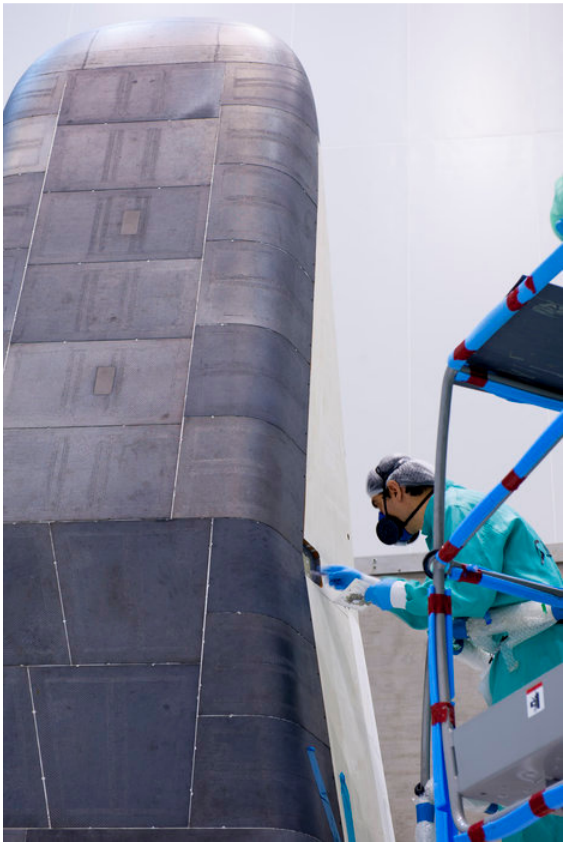

Figure 20: Last IXV ablative TPS tile being installed

7. Conclusions

IXV ablative TPS design involved several aspects of the engineering world. It has been a multidisciplinary program covering fields from very peculiar numerical simulations such as those on aerothermodynamics or dynamic environment, to material science problems to find the correct materials to fulfill the very demanding requirements, to technological difficulties to perform integration of hundreds of parts with required precision of a few tenth of a millimeter.

All these aspects have been managed through the integrated work of several teams involved in project and under the technical coordination of Thales Alenia Space Italy and European Space Agency.

The result has been the flawless flight performed on last 11th of February 2015. Now the effort will be in reviewing the huge amount of flight data in order to verify the correctness of the calculation models and of the technological choice.

References

[1] Roark's Formulas for Stress & strain.